Supporting Information

Fine-Tuning Surface Oxidation States of Ruthenium Nanoparticles to Enhance Hydrogen Electrode Reactions

Hao Zhao, Jiejie Li, Jian Zou, Yangchun Tan, Chi Chen, Bo Yang, Qingqing Cheng, Hui Yang**

Experimental methods

Chemicals and Materials

Ruthenium (III) 2, 4-pentanedionate ($Ru(acac)_3$,98%+), styrene (99%) and potassium thiocyanate (KSCN) were bought from damas-beta. Polyvinylpyrrolidone (PVP, K30) and potassium peroxodisulfate ($K_2S_2O_8$) were obtained from Sinopharm Chemical Reagent Co. Ltd. (Shanghai, China). Other chemicals were bought from Sigma-Aldrich. All reagents were used directly without further purification. Ultrapure water (Millipore Milli-Q grade) with a resistivity of 18.2 MΩ·cm was used in all the experiments.

Preparation of polystyrene (PS) template

Monodispersed PS spheres with different diameters were synthesized by a typical emulsion polymerization according to the reported work with some modifications (Table S6)[1]. Typically, for PS spheres with 180 nm, 30 ml of styrene monomer was washed thoroughly with 10 mL of 10 wt.% NaOH solution to remove the stabilizer. Then it was further washed with deionized water for three times to remove residual NaOH. Next, the faint yellow styrene monomer was added to 500 ml triple-neck containing 250 ml of ultrapure water and 1.5 g of PVP. After replacing with N_2 for several times, the mixture was fluxed at 75°C under 450 rpm under N_2 atmosphere for 30 min. Subsequently, 25 ml of aqueous solution containing 500 mg of $K_2S_2O_8$ was injected into the flask to initiate the polymerization of styrene. After keeping at 75°C

and 450 rpm for 24 h, the milk-like suspension was centrifuged at 6000 rpm for 10 h and the product was dried at 60°C overnight to get the ordered PS template.

Preparation of Ru-NPs/OPC-Xnm

8.15 g of $Zn(NO_3)_2 \cdot 6H_2O$, 112 mg of $Ru(acac)_3$, and 6.75 g of 2-methylimidazole were dissolved in 45 mL of methanol solution successively. After stirring for 15 min, the PS template (d≈180 nm) was immersed in this solution for 1 h and further treated by vacuum degassing for another 1 h. The impregnated PS template was taken out and dried at 50 °C for 6 h. Then, the dried PS template was immersed into a mixed solution of methanol and ammonia (volume ratio: 2:1) for 24 h to initiate rapid growth of ZIF-8 inside the PS template, to form the $Ru(acac)_3$@ZIF-8@PS. After washing with DMF for six times, the sample was dried and calcined at the certain temperature under H_2/Ar flow for 3 h with a ramp rate of 5 °C min^{-1} (900°C: 0.9 nm, 950°C: 1.9 nm, 1000°C: 2.9 nm, 1025°C: 4.2 nm, 1050°C: 5.3 nm and 1100°C: 8.7 nm, respectively).

Preparation of pure OPC support

The synthesis method of pure OPC is similar to that of Ru-NP/OPC-X nm but without adding $Ru(acac)_3$ in the precursor's solution.

Preparation of C-Ru-NPs derived from conventional 1.5 µm ZIF-8

For a comparison, C-Ru-NPs without ordered porous structure was also synthesized according to the previously published work with some modifications.[2] Typically, 3.39 g of $Zn(NO_3)_2$ $6H_2O$ and 93 mg of $Ru(acac)_3$ were dissolved into 35 ml of methanol and another 35 ml of methanol solution containing 3.94 g of 2-methylimidazole was prepared. After mixing the solutions, the solution was refluxed at 60°C for 24 h without stirring. The pink precipitant was collected and washed with ethanol for 3 times, then the product was dried at 60°C in a vacuum oven. To this end, $Ru(acac)_3$@ZIF-8 was subjected to calcine at a certain temperature under H_2/ Ar flow in a tube furnace to obtain C-Ru-NPs.

Electrocatalytic Measurements

Performance evaluation of the HER/HOR: The performance was evaluated by CHI 760E electrochemical station in a standard three-electrode system, using a carbon rod as the counter electrode, a saturated Hg/Hg_2SO_4 electrode as the reference electrode (in saturated K_2SO_4 solution) and a glassy carbon electrode (GC, 5 mm in diameter) as the working electrode. The GC electrode was polished with alumina powder (0.3μm and 0.05μm) for 10 min before using. However, all the potentials in this work are given relative to the reversible hydrogen electrode (RHE). The ink which consisted of 600 μL of EtOH, 360 μL of H_2O, 40 μL of 5 wt% Nafion solution and 8 mg of catalyst was ultrasonicated for at least 2 h under ice bath. Then 20 μL of this well-dispersed catalyst ink was dropped on pre-polished GC disk and dried with infrared lamp under 300 rpm. Freshly made ink was used for each test. The HER and HOR were carried out in N_2-saturated 0.5 M H_2SO_4 and H_2-saturated 0.1 M $HClO_4$, respectively. The polarization curves were measured at 5 mV s^{-1} for the HER and 10 mV s^{-1} for the HOR with 85% iR compensation. The AC impedance was measured from 1×10^6 to 0.1 Hz at open circuit potential with the amplitude of 5 mV.

The underpotential deposition of copper (CuUPD): The working electrode with catalyst was firstly cycled in N_2-saturated 0.5 M H_2SO_4 solution between 0.05 and 0.85 V versus RHE. After stabilization, linear sweep voltammetry (LSV) from the optimized potential to 0.85 V was performed with a scan rate of 10 mV s^{-1} as the background. Then the electrode was transferred into the N_2-saturated 0.5 M H_2SO_4 solution containing 5 mM $CuSO_4$ for CuUPD and polarized at the optimized potential for 100 s to form the monolayer Cu. Finally, the LSV was recorded under the same conditions. The number of active sites (n), turnover frequency (TOF) and electrochemical active surface area (ECSA) can be calculated by following equation based on CuUPD.

$$Q_{Cu} = \frac{1}{v}\left(\int I_{CuSO_4} \cdot dV_{CuSO_4} - \int I_{H_2SO_4} \cdot dV_{H_2SO_4}\right) \quad (1)$$

Where Q_{Cu} is the stripping charge of monolayer Cu (CuUPD → Cu^{2+} + 2e), v is the

scan rate. I and V is the current and potential during CuUPD.

$$n = Q_{Cu}/2F \quad (2)$$

Where n is the number of active sites and F is the Faraday constant (C mol^{-1}).

$$TOF = I/(2Fn) \quad (3)$$

Where I is the current (A) during linear sweep measurement, F is the Faraday constant (96485 C mol^{-1}). The factor 1/2 is based on the consideration that two electrons were required to form one hydrogen molecule.

$$ECSA_{Cu} = Q_{Cu}/420\ \mu C \cdot cm^{-2} \quad (4)$$

Where $420\mu C \cdot cm^{-2}$ the maximum packing charge density of Cu on Ru.

Characterizations

The crystalline structure was determined by Bruker D8 ADVANCE powder X-ray diffractometer (PXRD) with Cu Kα radiation (λ = 1.5418 Å). The morphology and size of the catalysts were observed by field-emission scanning electron microscope (FESEM, Regulus8100, accelerating voltage: 5 kV) and transmission electron microscope (TEM, JEM-2100F and Tecnai G2 F30 S-Twin, accelerating voltage: 200 kV). Atomic-scale structure was observed via spherical aberration corrected transmission electron microscope (AC-TEM, JEM ARM 200F, accelerating voltage: 200 kV). The N_2 sorption experiments were performed using Micromeritics ASAP 2020 at 77 K. The metal contents of the catalysts were analyzed using inductively coupled plasma-optical emission spectrometer (ICP-OES, Agilent ICPOES730). X-ray photoelectron spectroscopy (XPS) was conducted on Thermo-scientific ESCALab 250Xi. Thermal gravimetric analyzer (TGA) data were recorded by Q5000. X-ray absorption fine structure spectra (XAFS) were collected at BL14W1 station in Shanghai Synchrotron Radiation Facility (SSRF), which operated at 3.5 GeV with a maximum current of 250 mA. The data were collected in transmission mode for Ru foil and RuO_2, and in fluorescence excitation mode for synthesized typical samples.

DFT Calculation

All the density functional theory (DFT) calculations were performed with the Vienna Ab-initio Simulation Package (VASP) code.[3] The electron-ion interaction was modeled with the projected augmented wave (PAW) method.[4] Perdew-Burke-Ernzerhof (PBE) functional[5] was used to approximate exchange and correlation energies. The energy cutoff was set as 400 eV and the convergence criteria for force was 0.05 eV/Å. The vacuum height was at least 13 Å to prevent the interaction between periodic structures. For each adsorbate, the energy of most stable configuration was used for free energy calculations. For Ru(0001) surface, it was constructed with a four-layer 3×3 slab with the topmost two Ru layers relaxed, and 4×4×1 k-point grid generated with the Monkhorst-Pack scheme was used.[3b] For RuO_2(110) surface, a four RuO_2 layered 1×2 slab was used with the topmost two RuO_2 layers relaxed, using 4×4×1 k-point grid. For the interface model of Ru-RuO_2 as shown in Figure S30, it was constructed with one-layer of RuO_2 binding on three-layer Ru(0001) with the topmost two Ru layers relaxed, and the k-point grid with 2×2×1 was used. Computational hydrogen electrode (CHE) method[6] was used for HER and HOR reaction free energy calculation. Entropies for gaseous H_2 (-0.40 eV) at 298.15K were used to correct the DFT energies into free energies, which can be obtained from NIST database.[7]

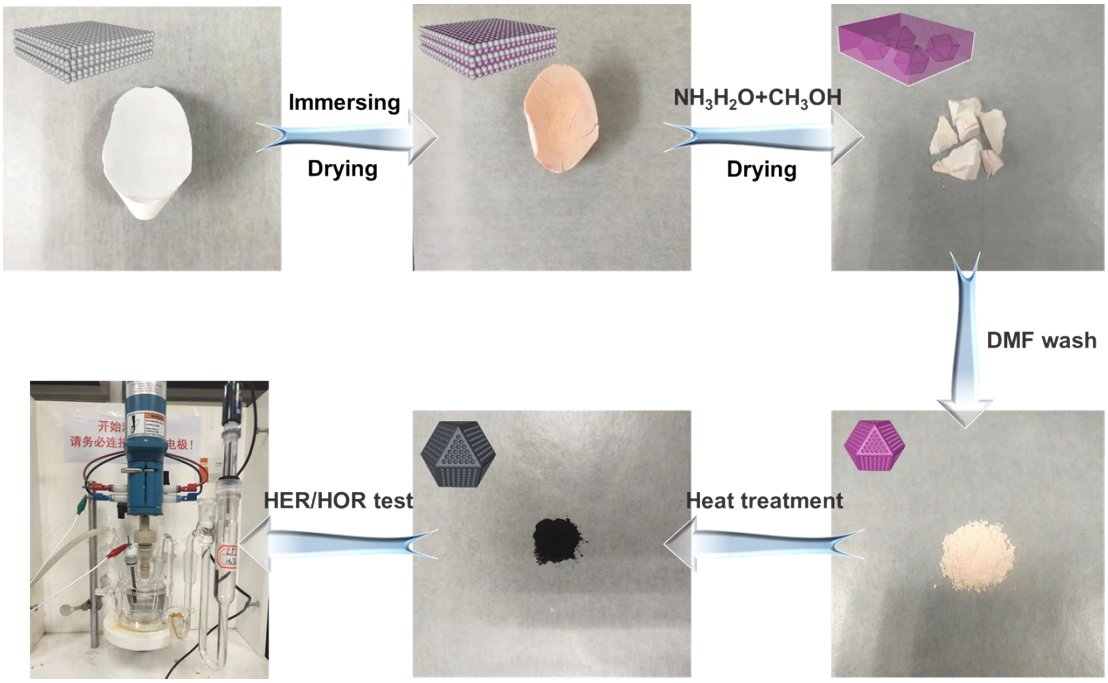

Figure S1. The photographs of sample statuss during the preparation procedure of Ru-NPs/OPC-X nm.

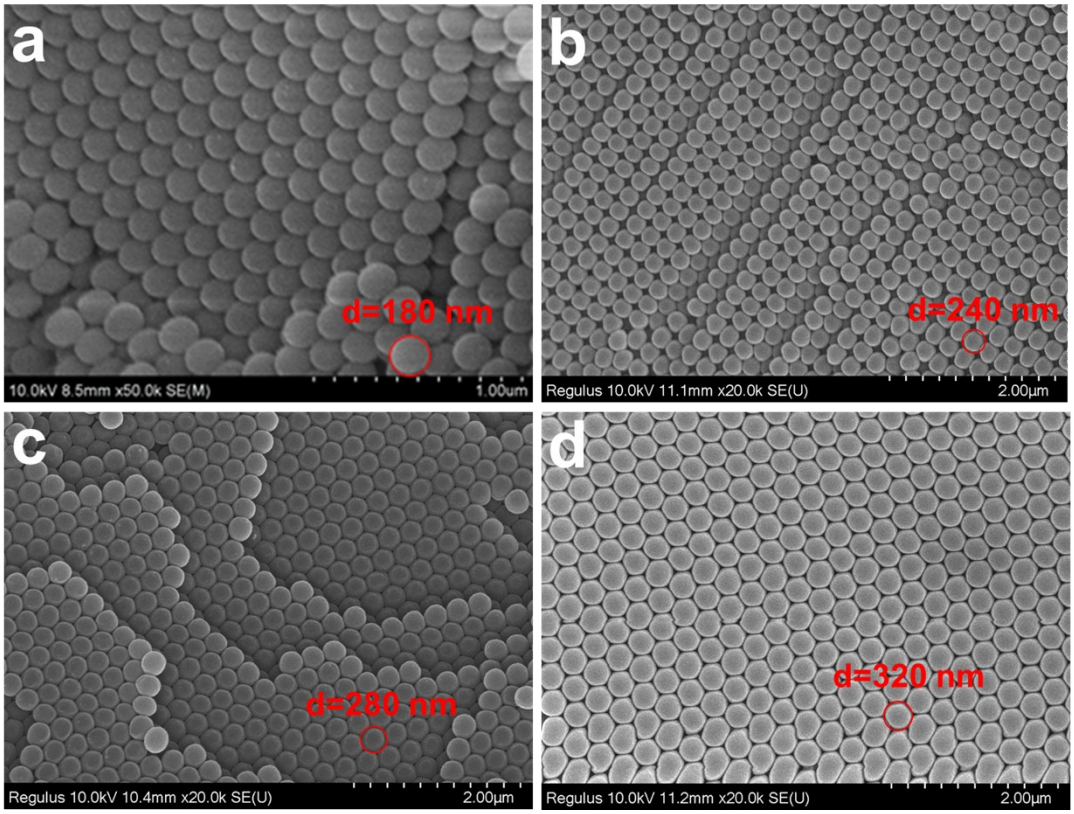

Figure S2. SEM images of PS template with different sizes: (a) d=180 nm; (b) d=240 nm; (c) d=280 nm; (d) d=320 nm. The PS template with an average diameter of 180 nm was chosen for Ru-NPs/OPC-X nm.

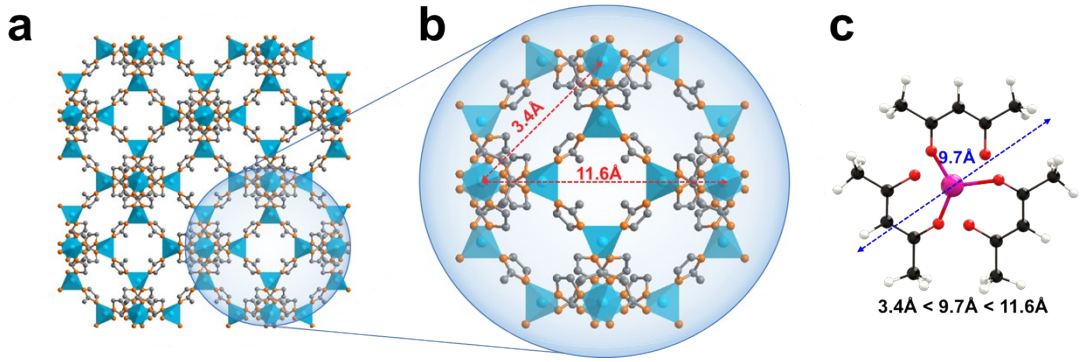

Figure S3. (a) Perspective view of single crystal ZIF-8; (b) Single cell of ZIF-8 with cavity diameter of 11.6 Å and pore diameter of 3.4 Å. (c) The molecular structure of $Ru(acac)_3$ with diameter of 9.7 Å.

The inherent structure of ZIF-8 allows $Ru(acac)_3$ being captured within the cage facilely because the diameter of $Ru(acac)_3$ is in between the cavity and the pore scale of ZIF-8. (C: grey/black, N: orange, Zn: blue, H: white, O: red, Ru: pink)

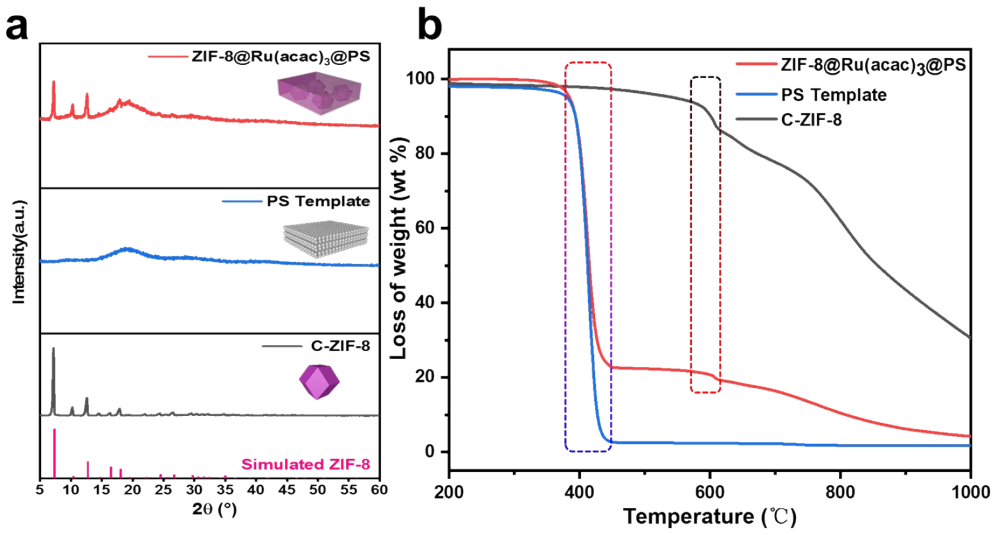

Figure S4. (a) XRD patterns and (b) TGA curves in nitrogen atmosphere of ZIF-8@Ru(acac)$_3$@PS, pure PS template and conventional ZIF-8.

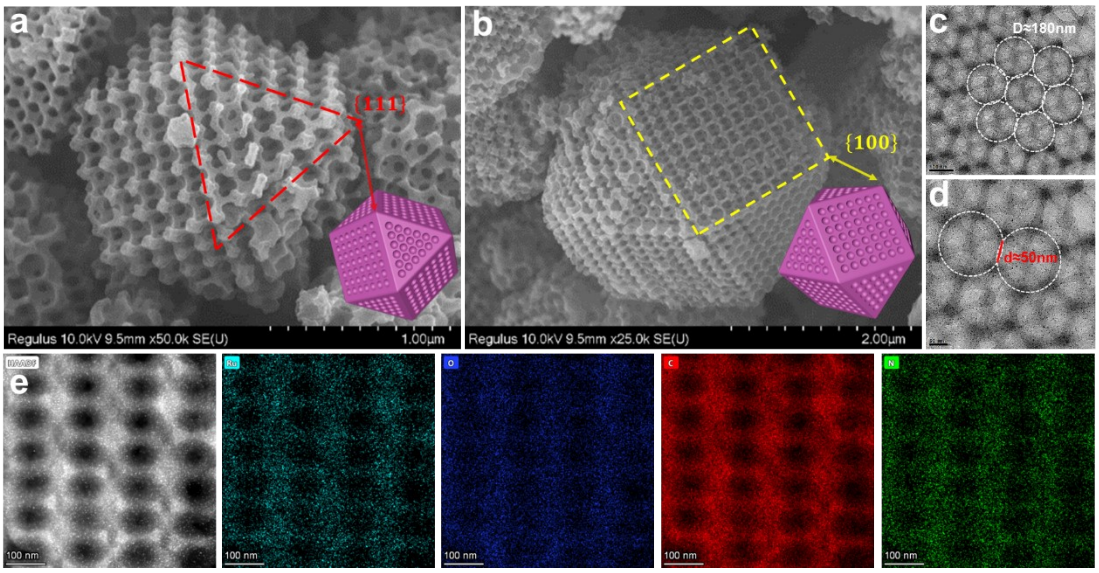

Figure S5. (a, b) S E M images of individual crystal taken from two typical directions. (c-e) HRTEM, HAADF-STEM images of the pores structure and corresponding EDS elemental mappings of Ru, O, C, N.

As shown in Figure S5, the well-defined tetrakaidecahedron morphology is observed. Besides, the clear (111) and (100) facets witness the regular crystallization of hierarchical pore ZIF-8.

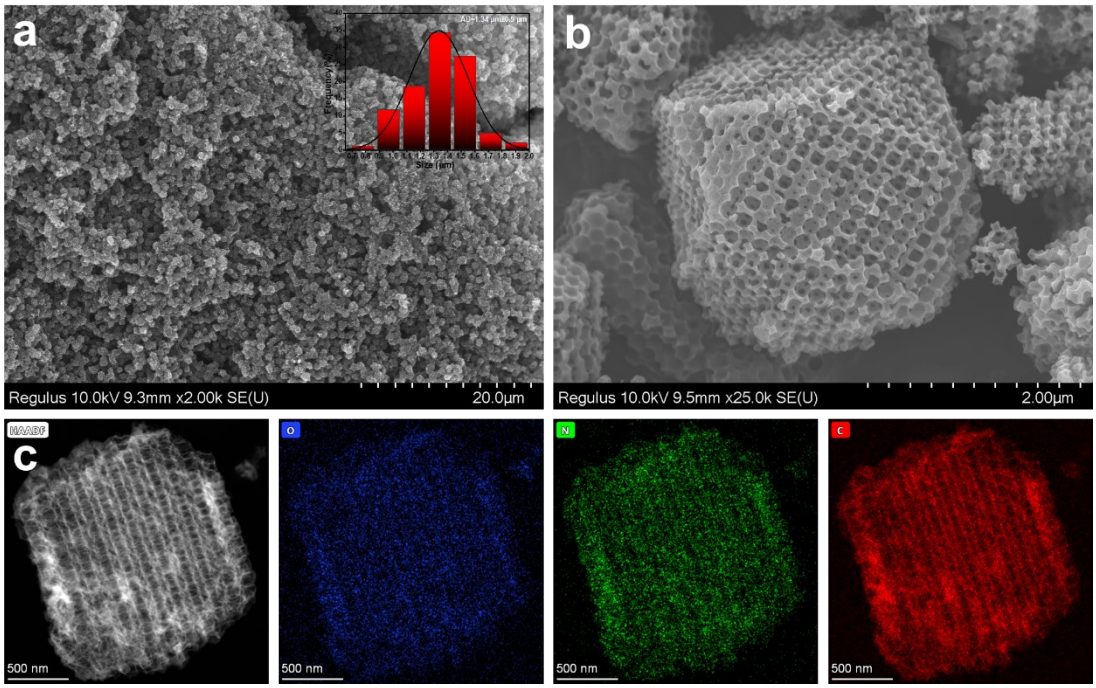

Figure S6. Morphology analysis of pure OPC support without Ru element. (a, b) SEM images at different magnifications. (c) HAADF-STEM image and corresponding EDS elemental mappings of O, N, C.

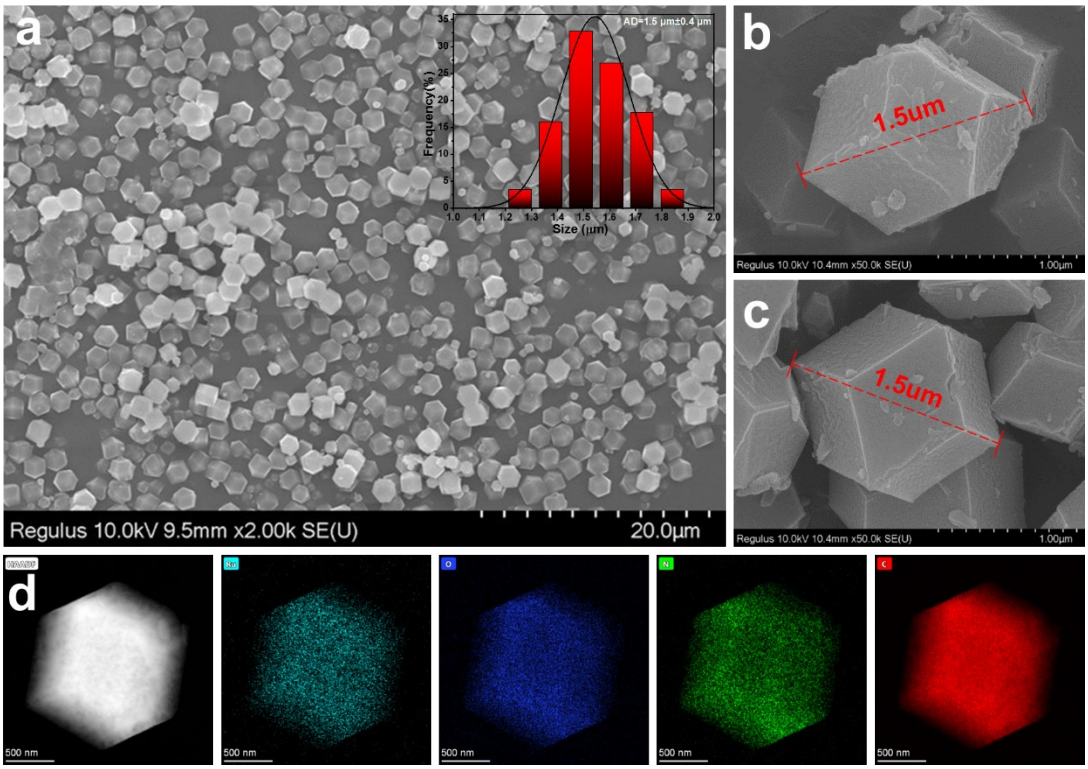

Figure S7. Morphology analysis of conventional Ru NPs exempt of interconnected macropores structure. (a-c) SEM images at different magnification. (d) HAADF-STEM image and corresponding EDS elemental mappings of Ru, O, N, C.

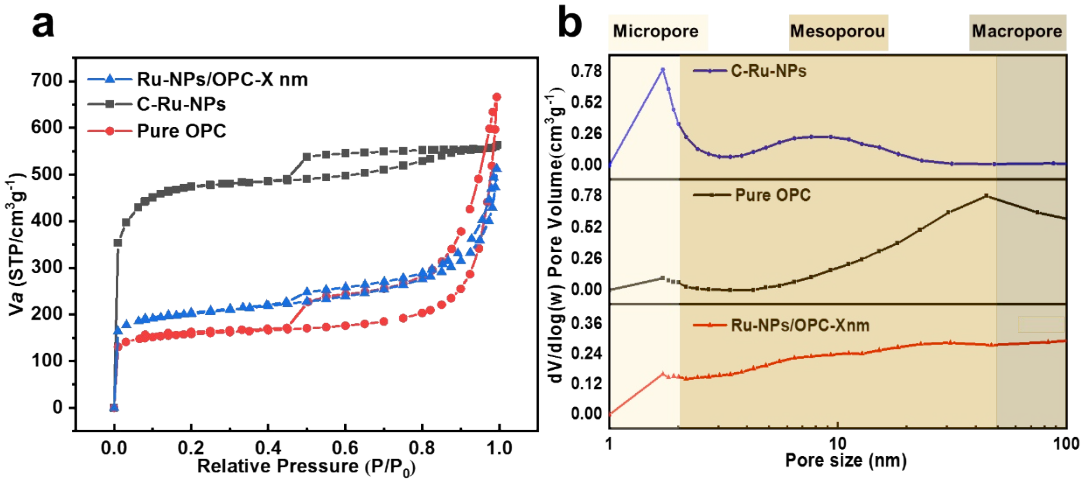

Figure S8. Ordered porous structure characterization of Ru-NPs/OPC-X nm and the comparative sample. (a) N_2 adsorption-desorption curves and (b) corresponding pore size distribution curves of Ru-NPs/OPC-X nm, C-Ru-NPs and pure OPC based on a method of BJH.

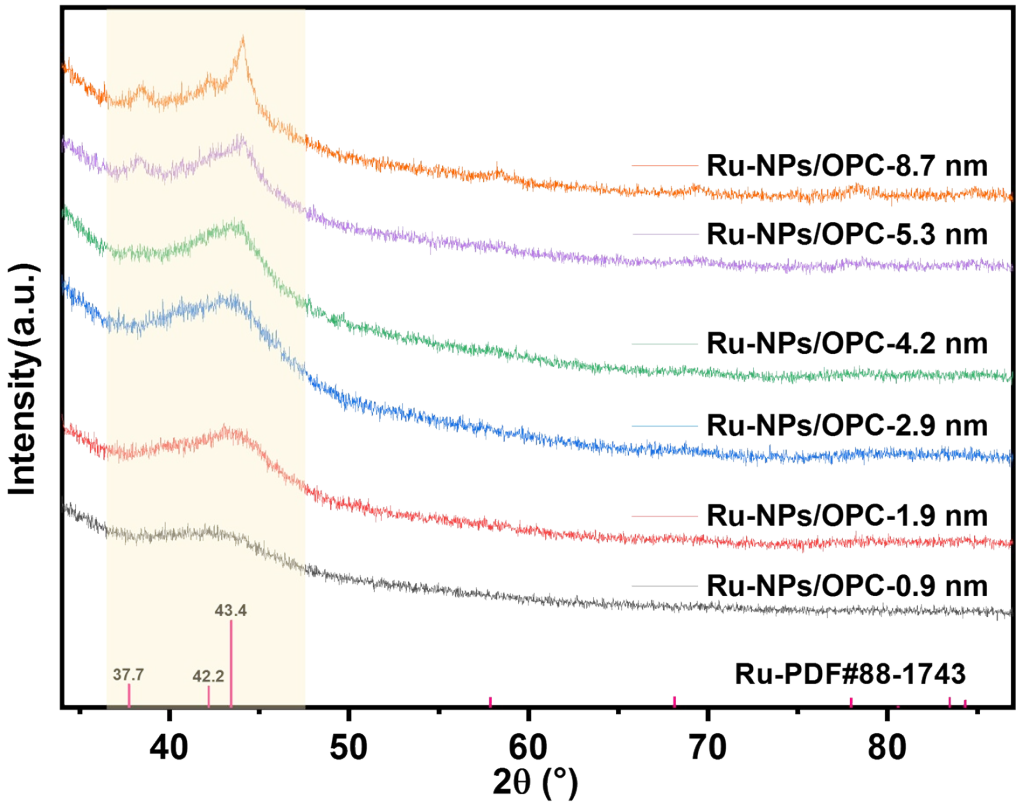

Figure S9. XRD patterns of Ru-NPs/OPC-X nm.

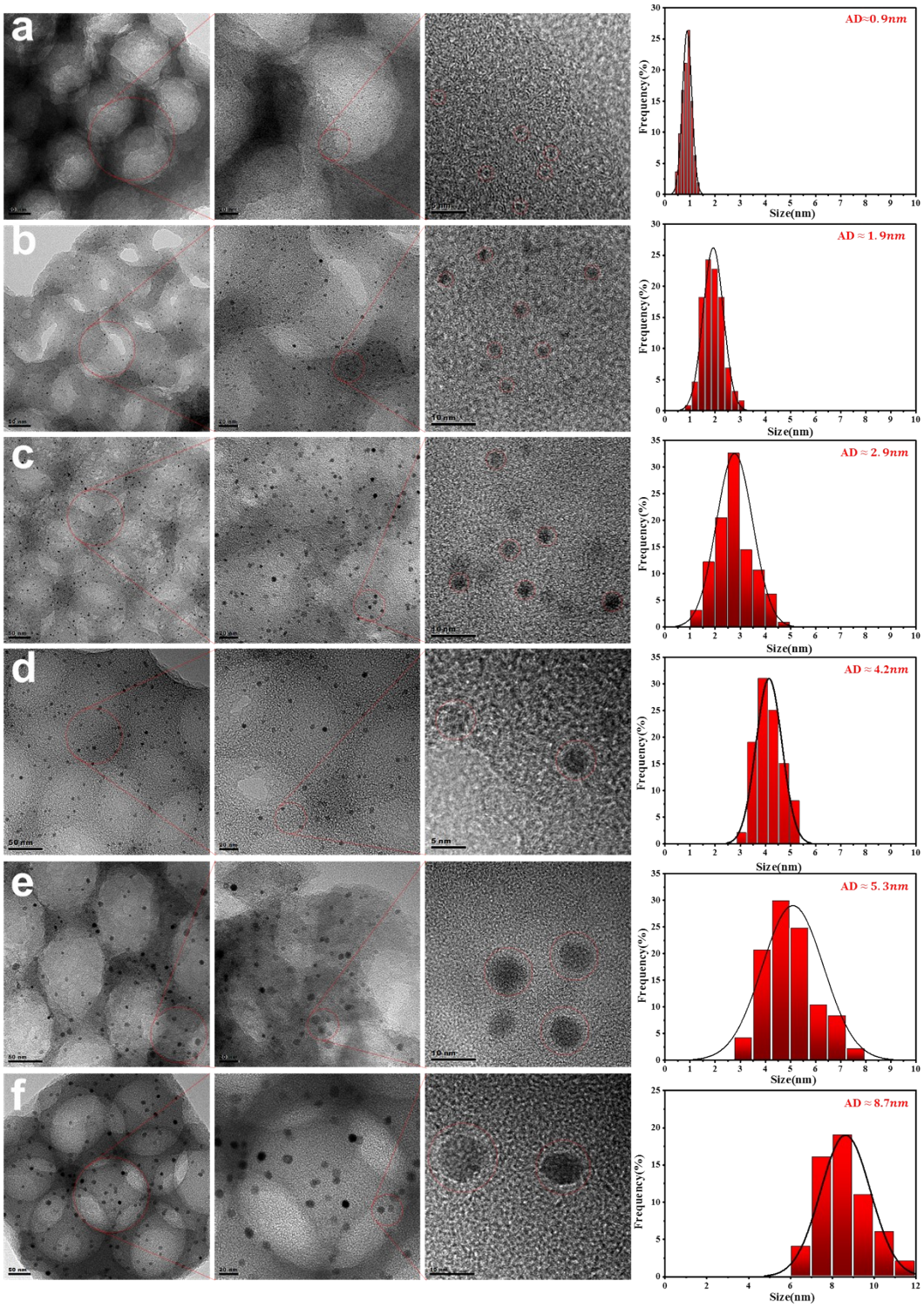

Figure S10. TEM, HRTEM images and size histograms of (a) Ru-NPs/OPC-0.9 nm, (b) Ru-NPs/OPC-1.9 nm, (c) Ru-NPs/OPC-2.9 nm, (d) Ru-NPs/OPC-4.2 nm, (e) Ru-NPs/OPC-5.3 nm and (f) Ru-NPs/OPC-8.7 nm.

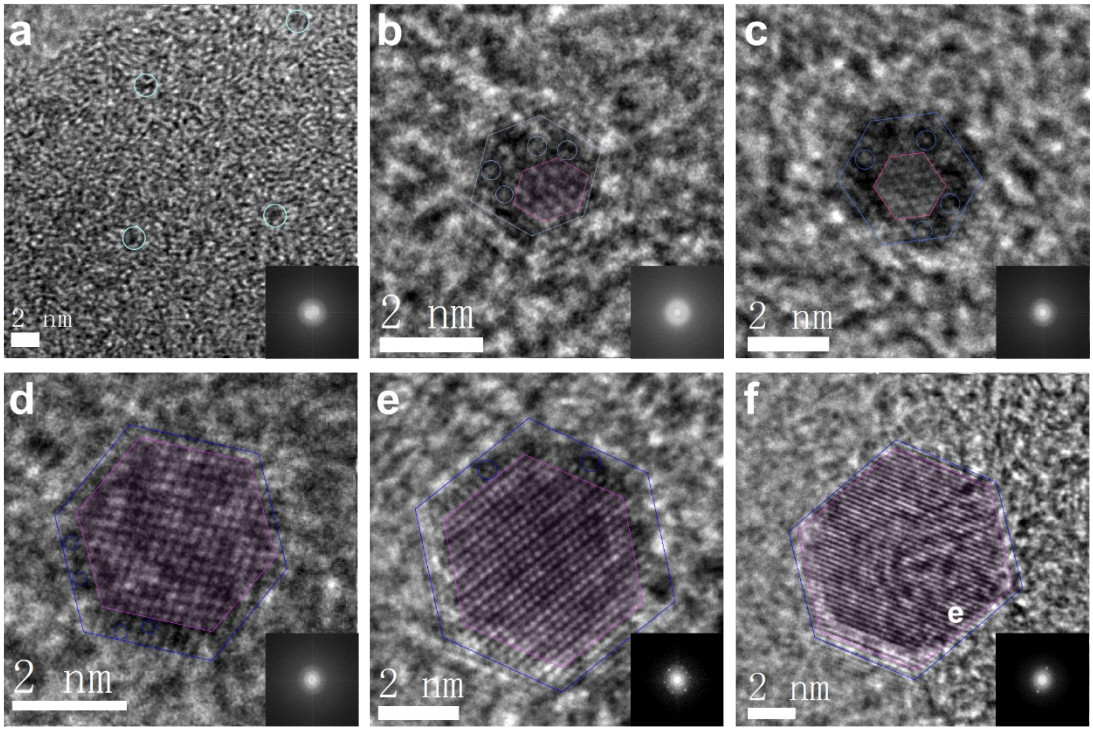

Figure S11. (a-f) HRTEM images of Ru-NPs/OPC-X nm from 0.9 to 8.7 nm (inset: corresponding fast Fourier transform images).

As seen in Figure S11 a-f, Ru NPs consist of crystalline Ru core (pink hexagon) and roughened surface (Blue hexagon). With the increase of crystallized Ru core, the roughened surface decreases gradually.

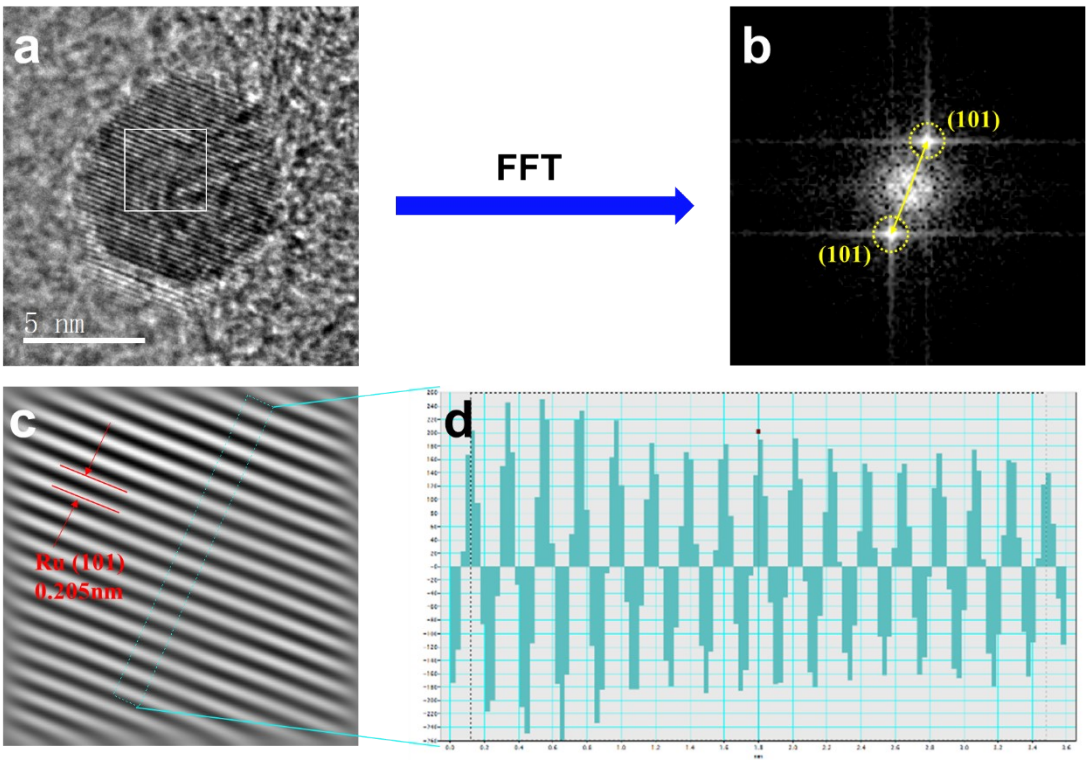

Figure S12. (a) HRTEM image of Ru-NPs/OPC-8.7 nm. (b) Fast Fourier transform (FFT) of (a). (c) Inverse FFT of (b). (d) Selected area atomic mass contrast distribution.

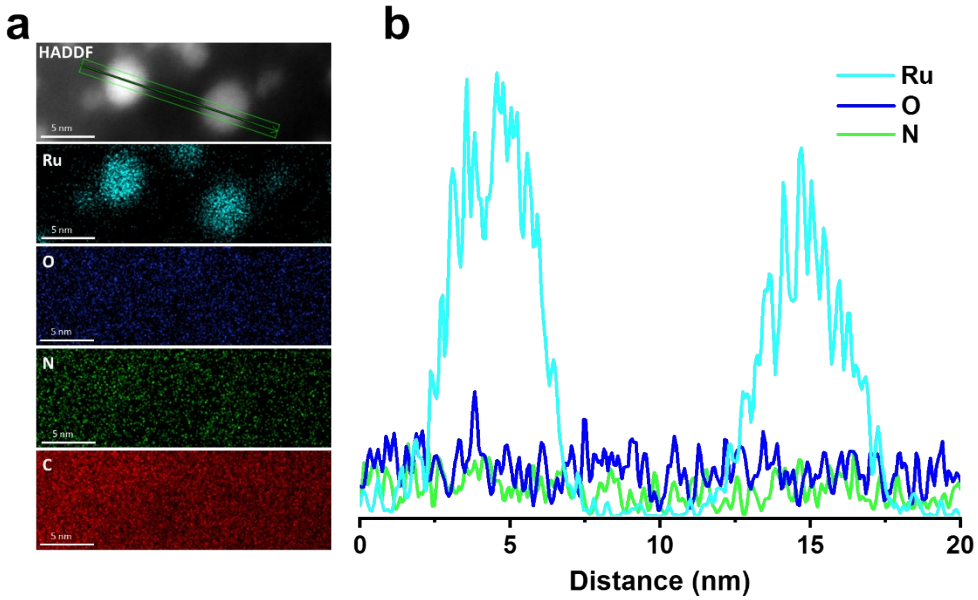

Figure S13. HADDF image of Ru NPs and corresponding (a) EDS mappings and (b) linear scan of Ru, N, O element.

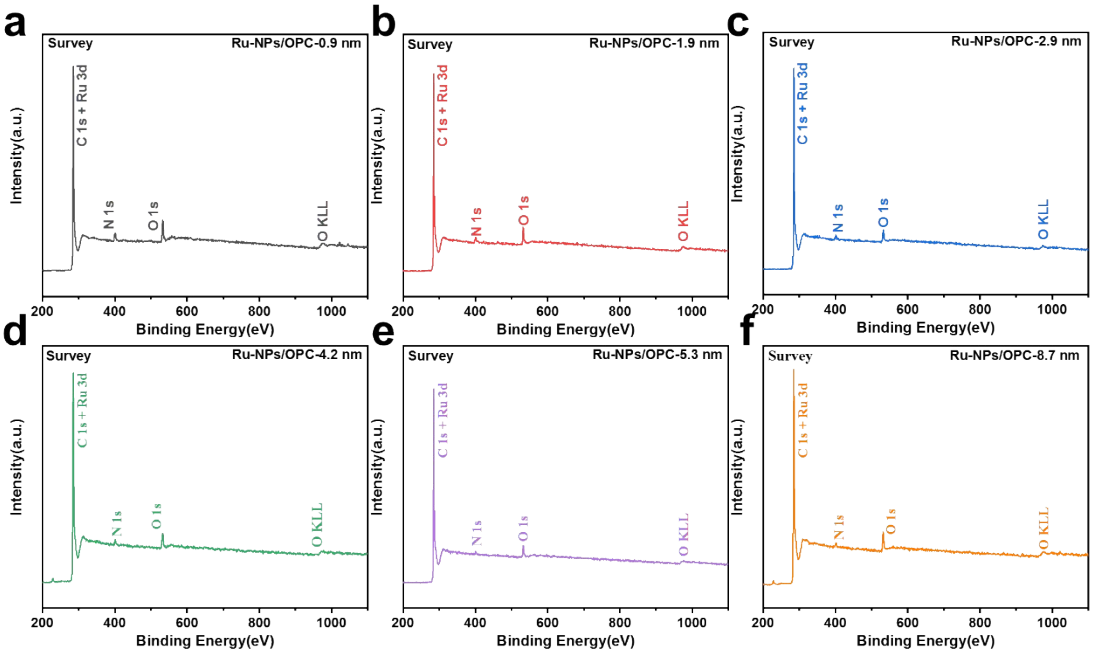

Figure S14. XPS survey spectra of Ru-NPs/OPC-X nm.

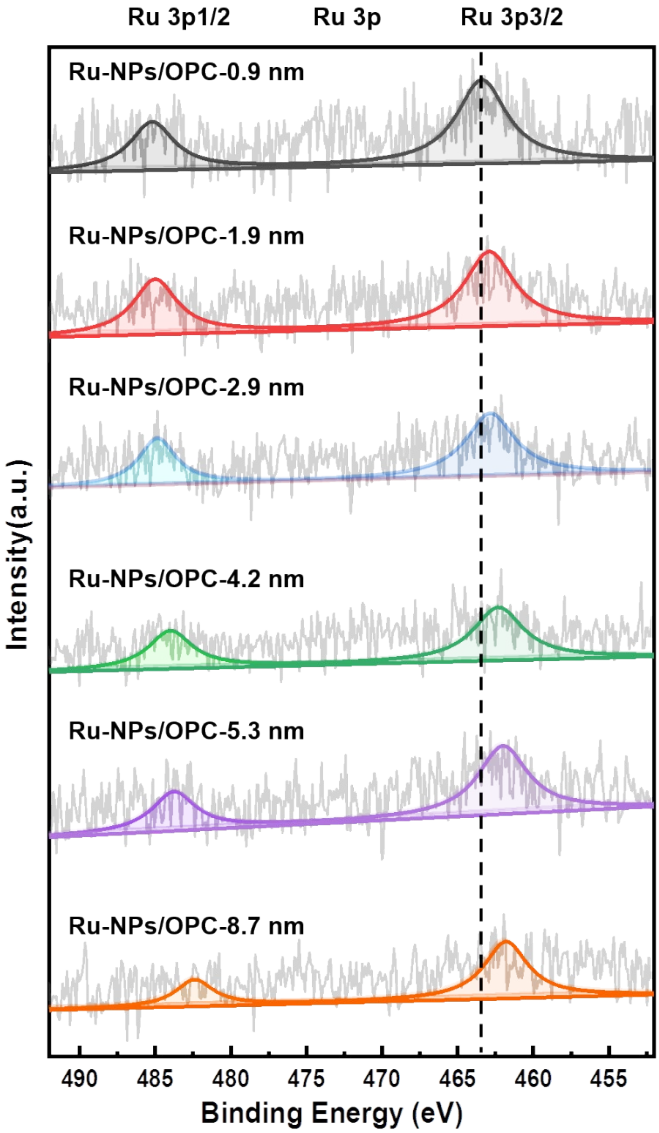

Figure S15. High-resolution XPS spectra of Ru 3p of Ru-NPs/OPC-X nm.

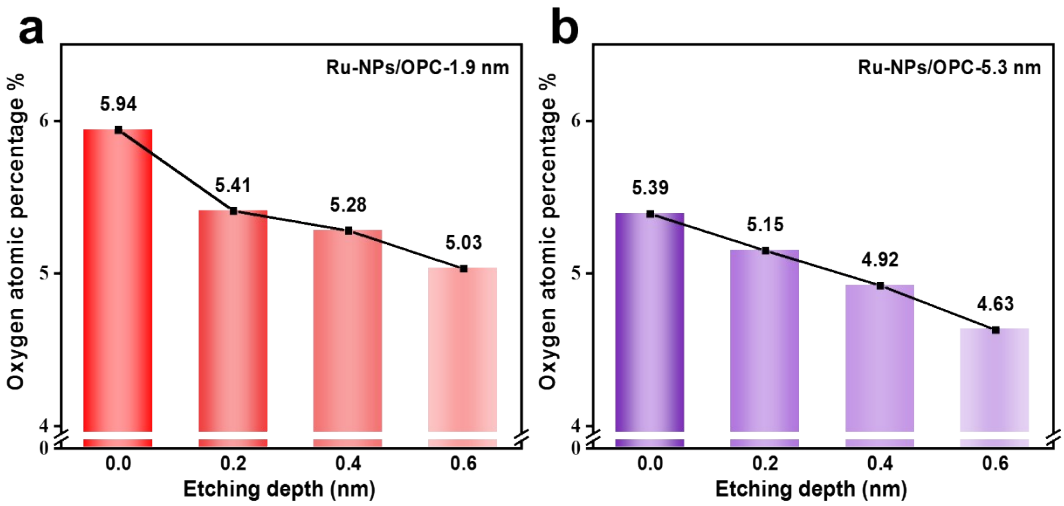

Figure S16. (a) The atom content of O at different etching depths for (a) Ru-NPs/OPC-1.9 nm and Ru-NPs/OPC-5.3 nm.

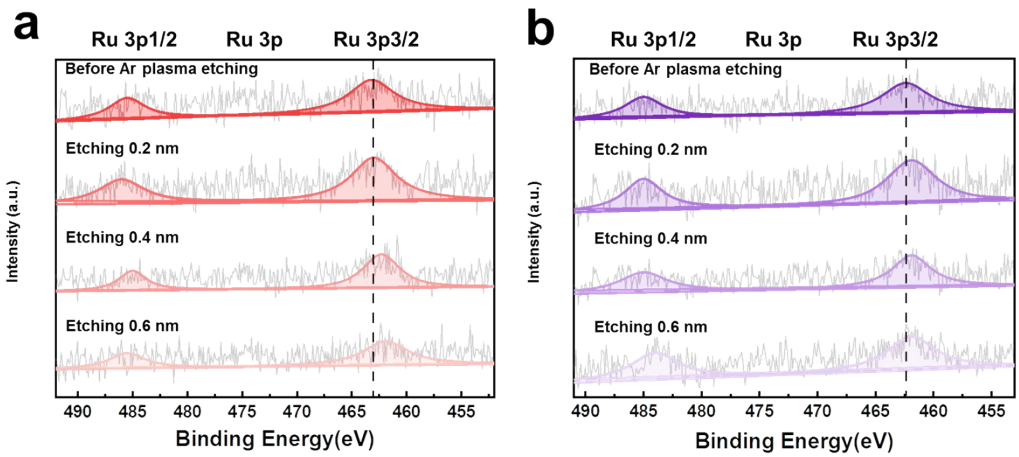

Figure S17. High-resolution XPS spectra of Ru 3p for (a) 1.9 nm and (b) 5.3 nm Ru-NPs after etching at different time.

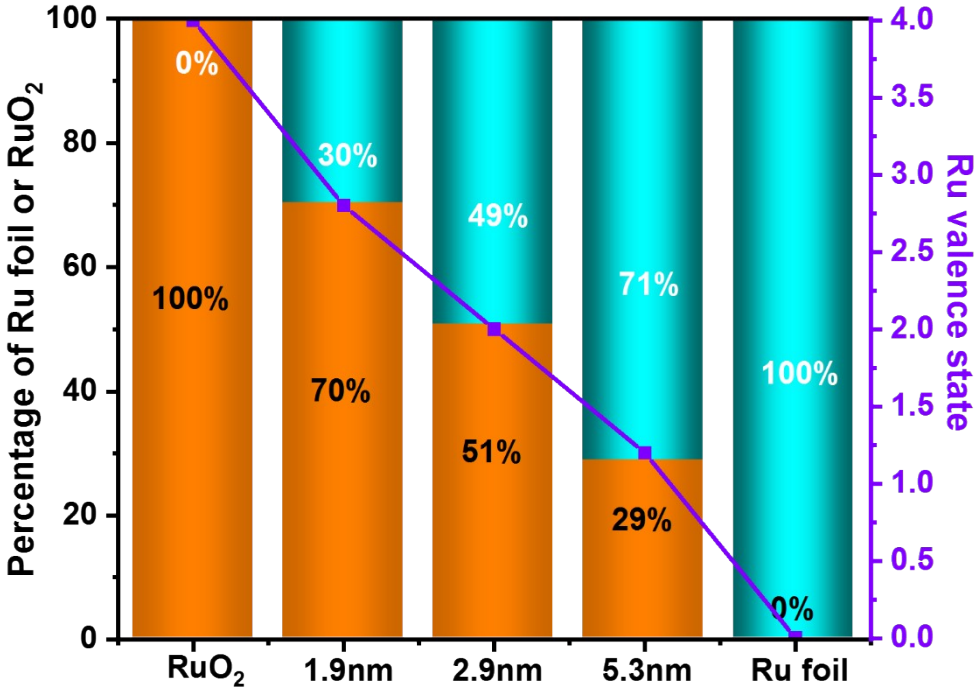

Figure S18. Linear component fitting of the typical samples.

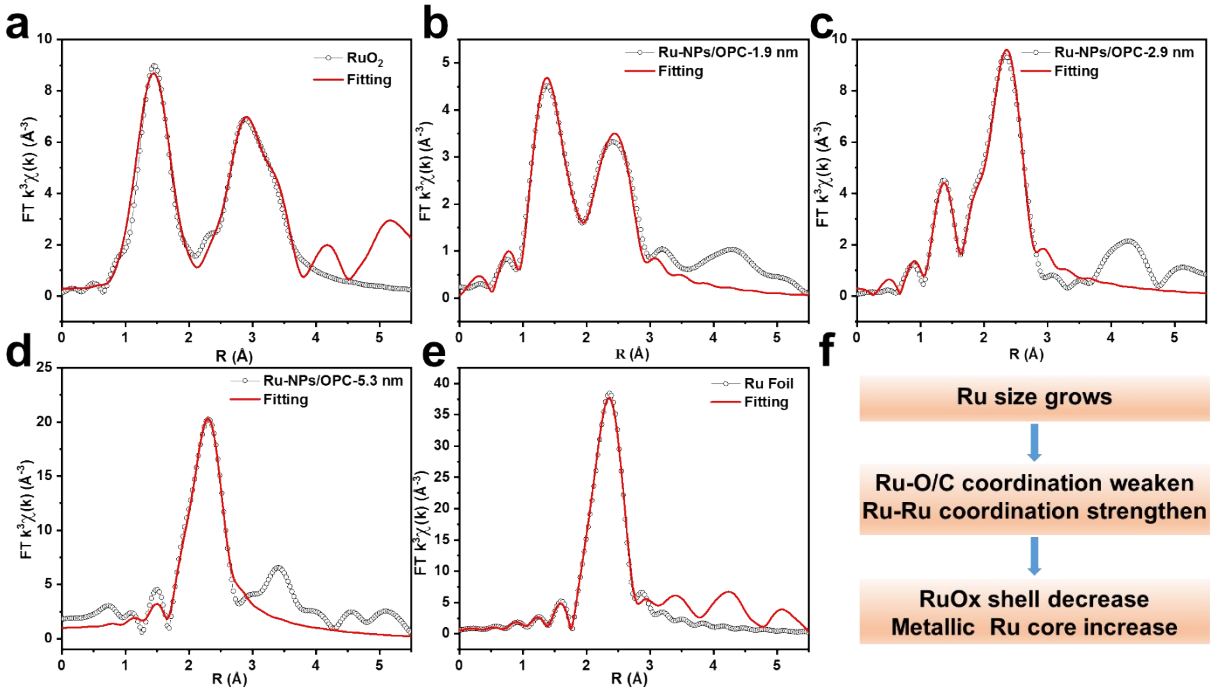

Figure S19. FT-EXAFS and corresponding R space-fitting curves of (a) RuO_2, (b) Ru-NPs/OPC-1.9 nm, (c) Ru-NPs/OPC-2.9 nm, (d) Ru-NPs/OPC-5.3 nm, (e) Ru foil. (f) Flow chart of the conclusion.

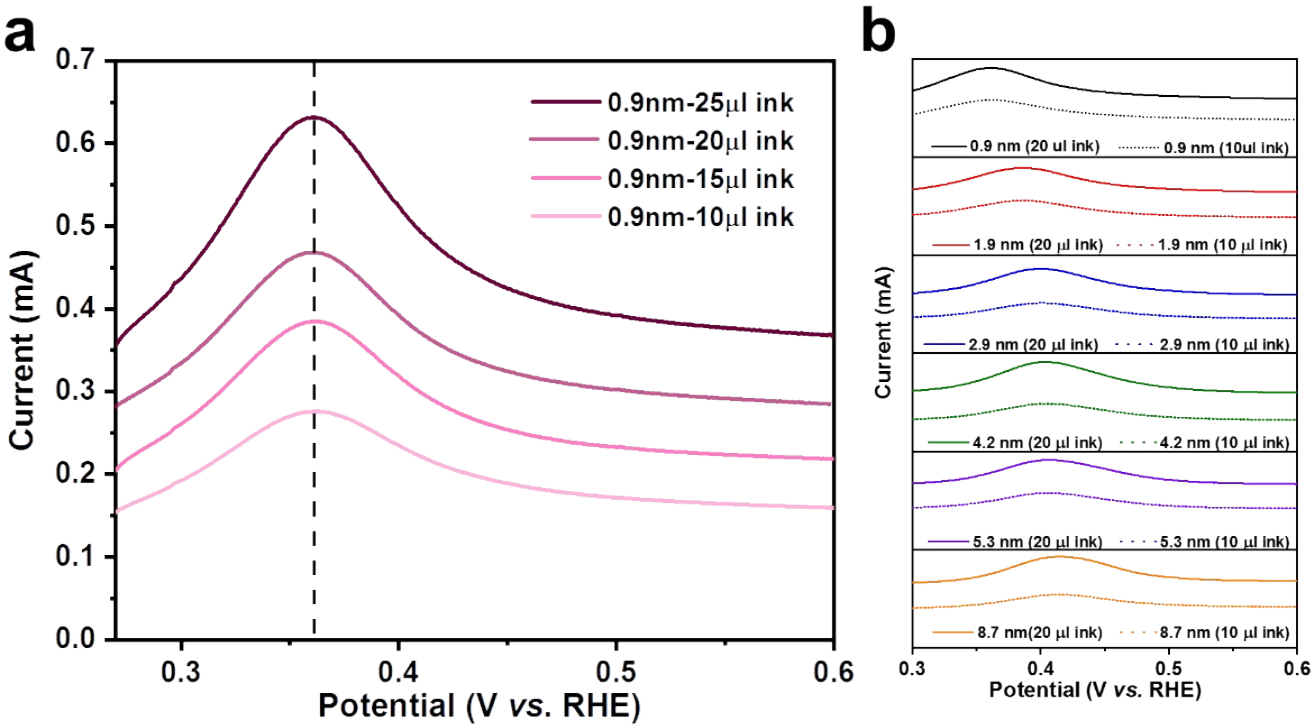

Figure S20 CuUPD stripping voltammetric curves of (a) Ru-NPs/OPC-0.9 nm with increasing Ru loading on working electrode and (b) Ru-NPs/OPC-X nm with various Ru sizes and loading.

CuUPD stripping voltammetric curves indicate the Ru-NPs possess the unique position of oxidation peak and the position is not affected by Ru loading, reflecting the intrinsic properties of the surface atoms.

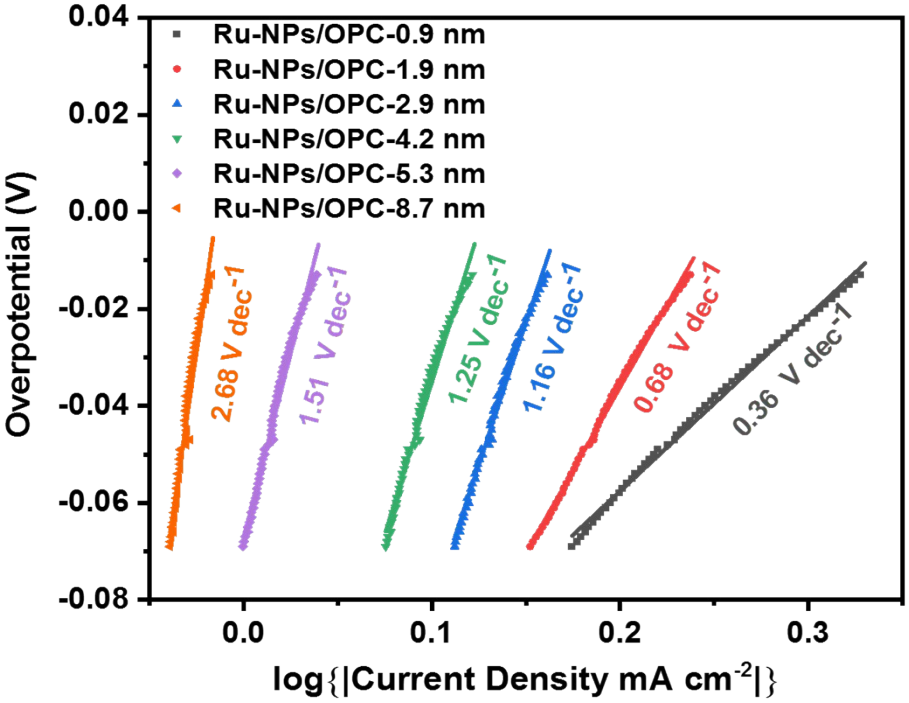

Figure S21. Tafel slopes for the electrooxidation of UPD Cu.

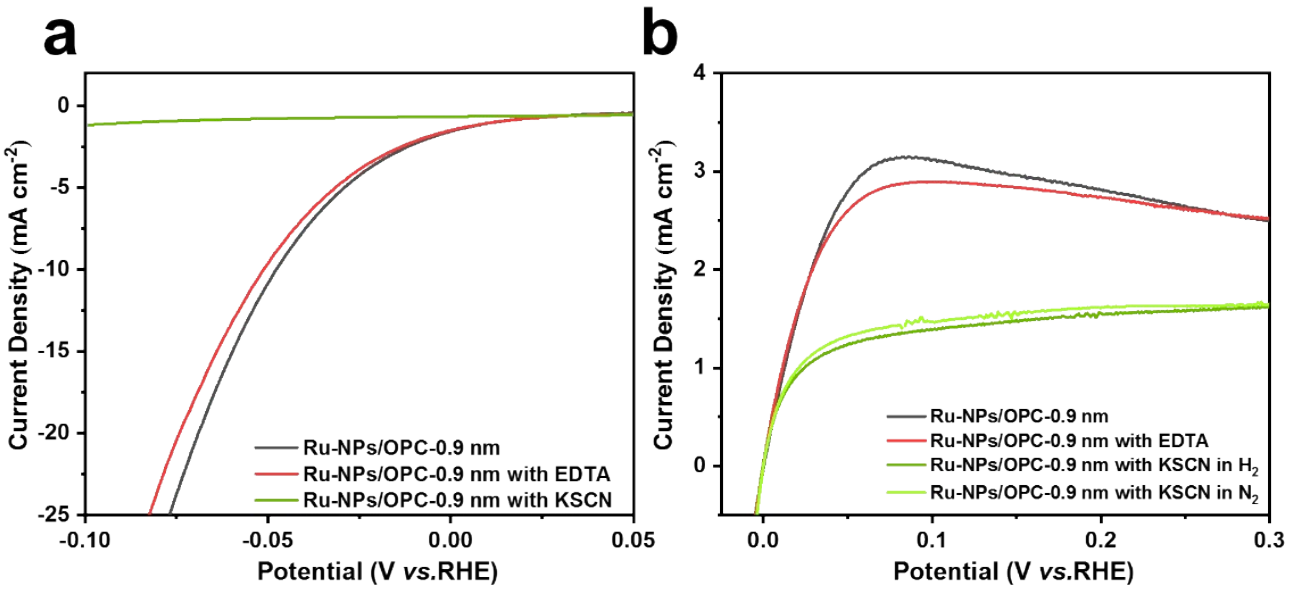

Figure S22. (a) Polarization curves for the HER on Ru-NPs/OPC-0.9 nm with the addition of EDTA (red line) and KSCN (green line). (b) Polarization curves for the HOR on Ru-NPs/OPC-0.9 nm with the addition of EDTA (red line) and KSCN (green line).

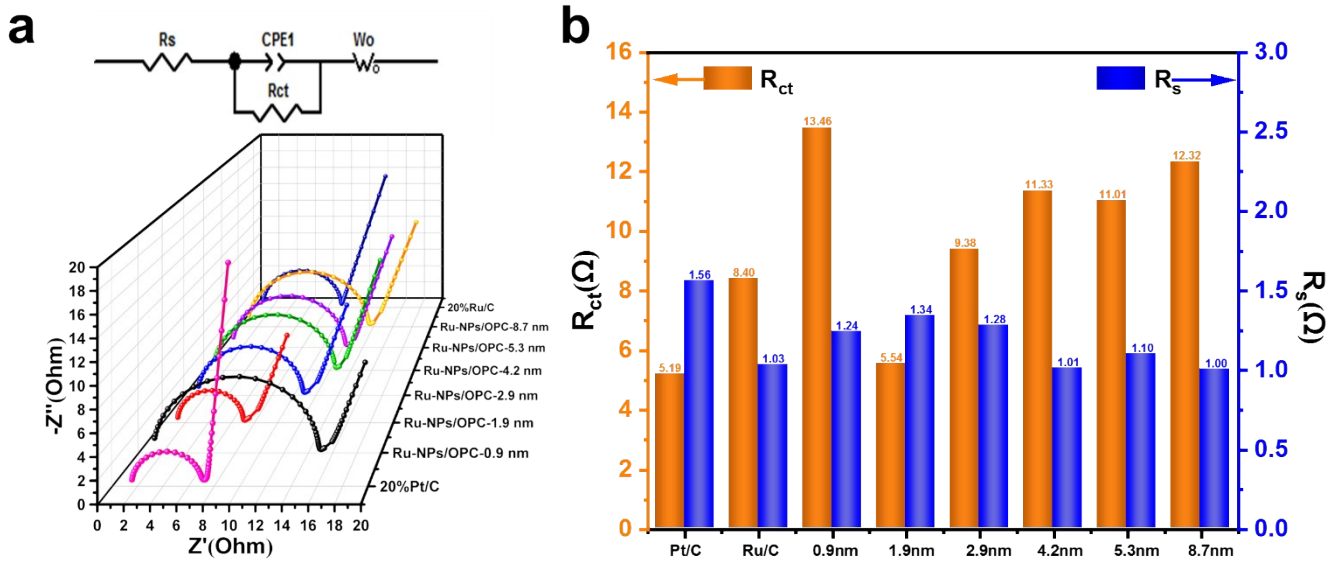

Figure S23. Electrochemical impedance spectroscopy (EIS) analysis of Ru-NPs/OPC-X nm. (a) 3D Nyquist plots of EIS (down) and corresponding equivalent circuit (top). (b) Calculated R_c and R_s according to the fitting results.

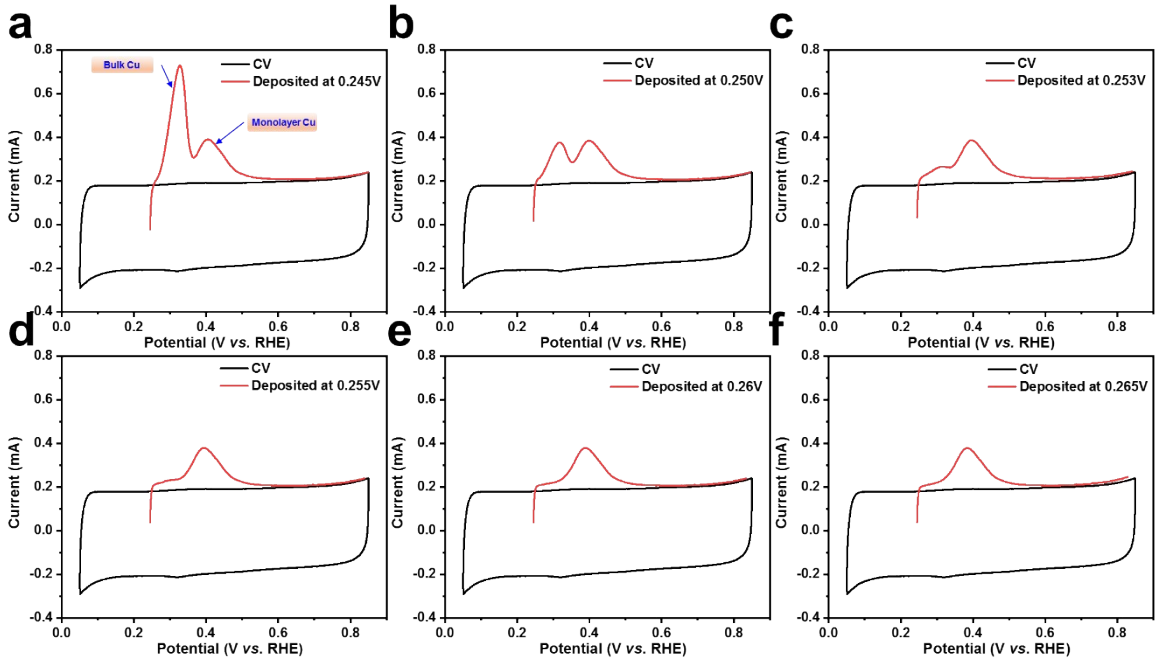

Figure S24. CuUPD on Ru-NPs/OPC-2.9 nm in 0.5 M H_2SO_4 in the absence (black) and presence (red) of 5 mM $CuSO_4$. For a-f, the electrode was polarized at 0.245, 0.250, 0.253, 0.255, 0.260 and 0.265 V for 100 s before electrooxidation, respectively.

As shown in Figure S24, Ru-NPs/OPC-2.9 nm was first polarized at 0.245, 0.250, 0.253, 0.255, 0.260 and 0.265 V for 100 s, respectively. As the potential rises from 0.245 to 0.265 V, the oxidation peak of bulk Cu at around 0.32 V falls gradually and that of monolayer Cu at near 0.40 V remains unchanged. To obtain the monolayer Cu, 0.26 V is selected in the following test of CuUPD.

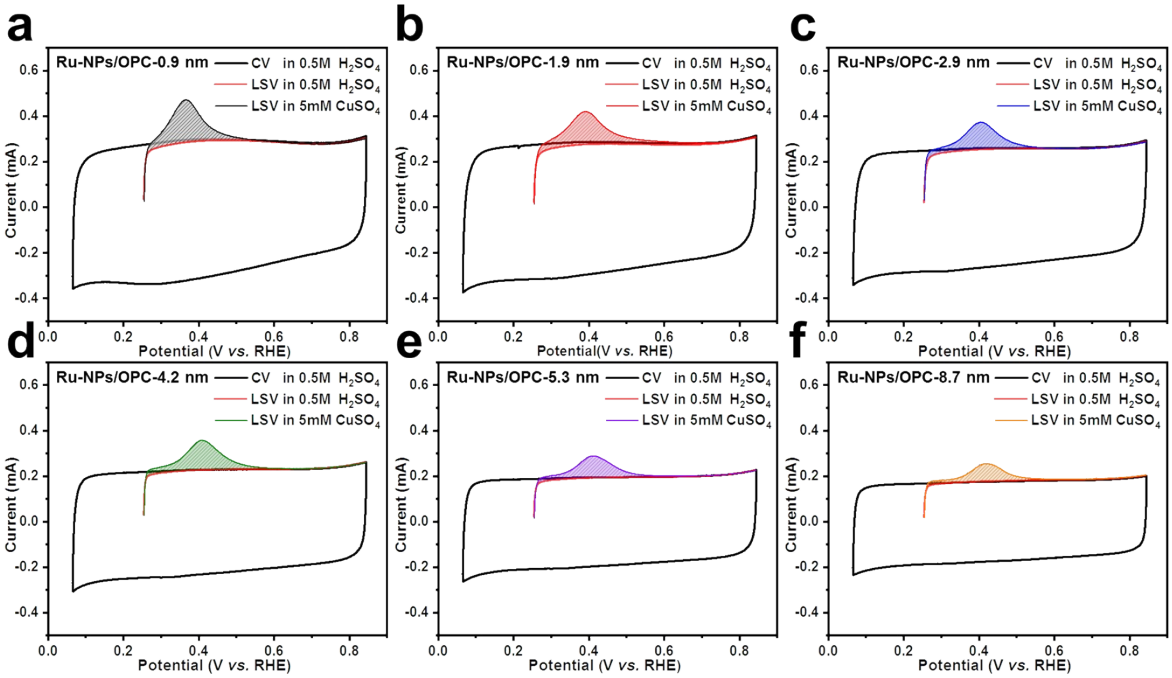

Figure S25. CuUPD in 0.5 M H_2SO_4 in the absence (red) and presence (chromatic) of 5 mM $CuSO_4$ on Ru-NPs/OPC-X nm. The electrode was polarized at 0.260 V for 100 s to form the monolayer Cu.

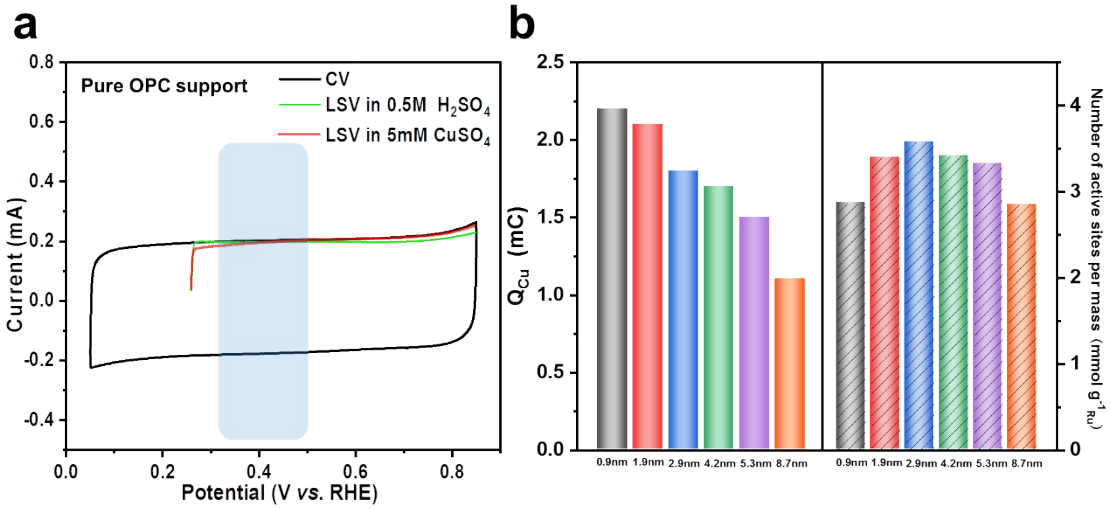

Figure S26. (a) CuUPD in 0.5 M H_2SO_4 in the absence (red) and presence (green) of 5 mM $CuSO_4$ on pure OPC support. (b) Charge transfer amount during CuUPD (left) and the number of active sites calculated from the CuUPD (right).

As shown in Figure S26a, no oxidation peak of monolayer Cu is observed, indicating that Cu^{2+} can be only underpotentially deposited on the surface of Ru-NPs rather than porous carbon supports, thus ensuring the accuracy of real area estimation. In Figure S26b, charge transfer amount during CuUPD and the number of active sites in Ru-NPs/OPC-X nm are calculated via equation (1) and (2) above.

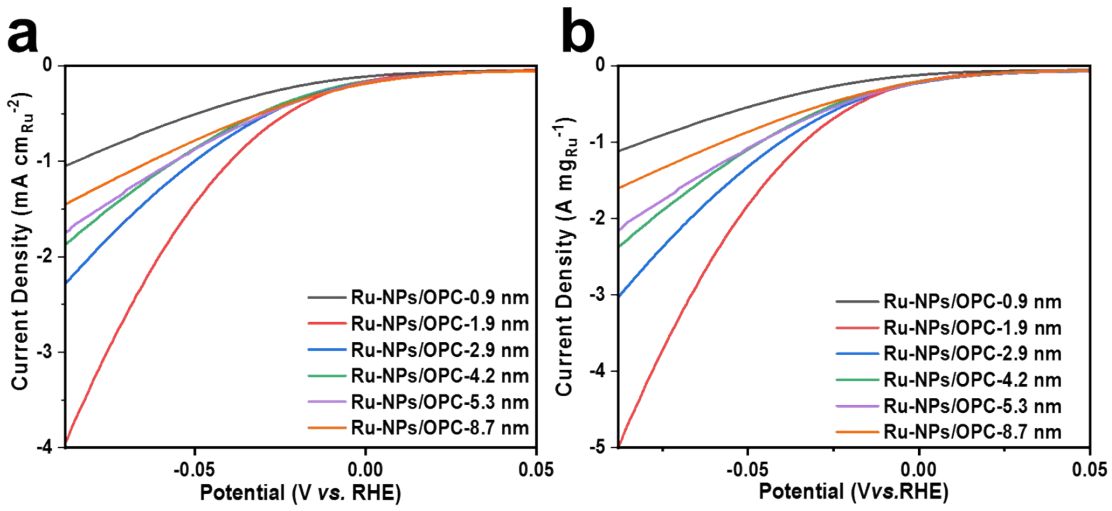

Figure S27. Specific activities (SA) and mass activities (MA) of the HER on Ru-NPs/OPC-X nm in 0.5M H_2SO_4.

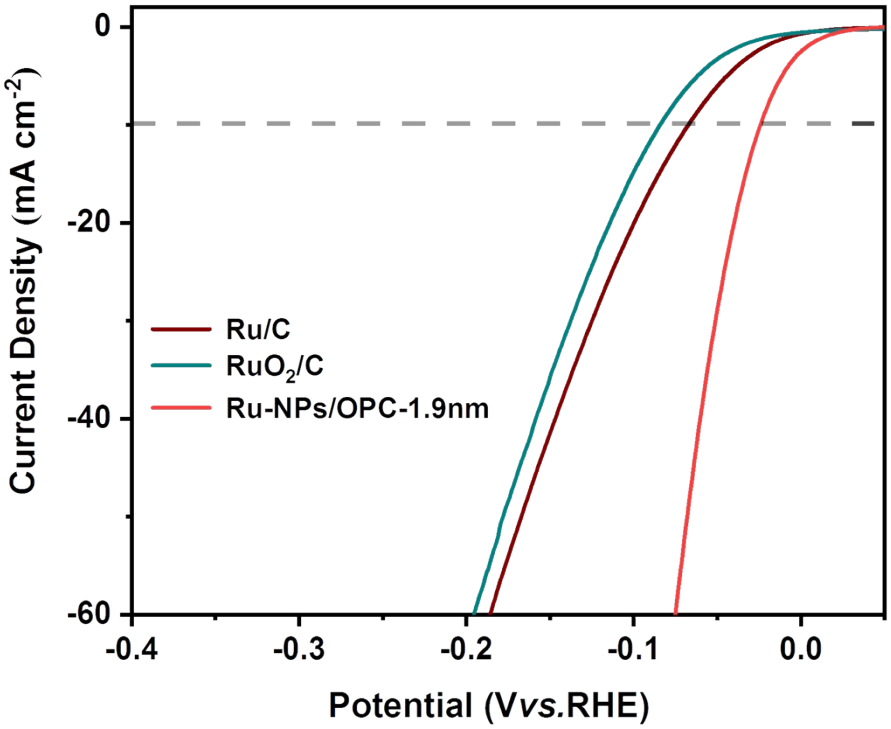

Figure S28. HER polarization curves on Ru-NPs/OPC-1.9 nm, Ru/C and RuO_2/C

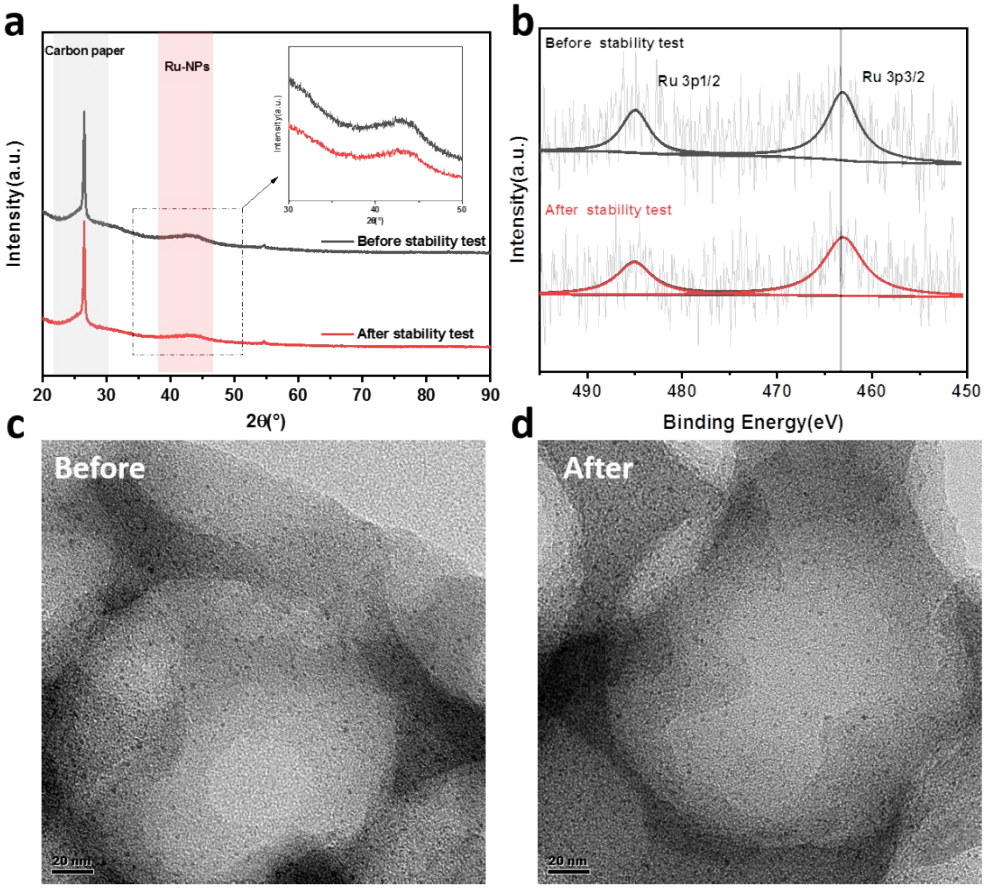

Figure S29. (a) XRD patterns, (b) XPS spectra, and (c, d) TEM images before and after HER stability testing.

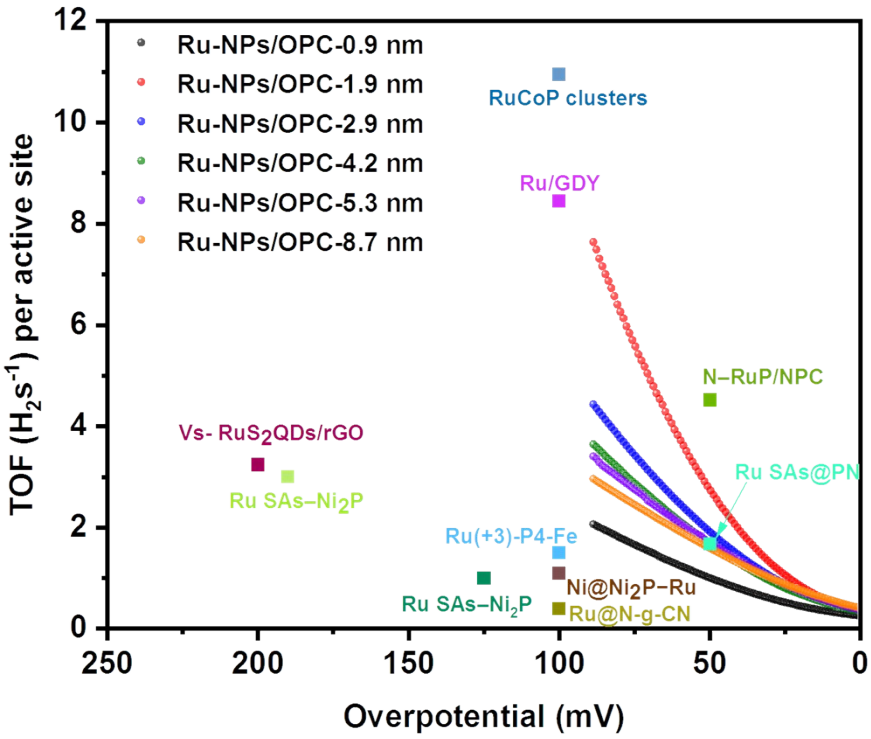

Figure S30. Comparison of TOF values between Ru-NPs/OPC-X nm and other HER electrocatalysts in 0.5M H_2SO_4.

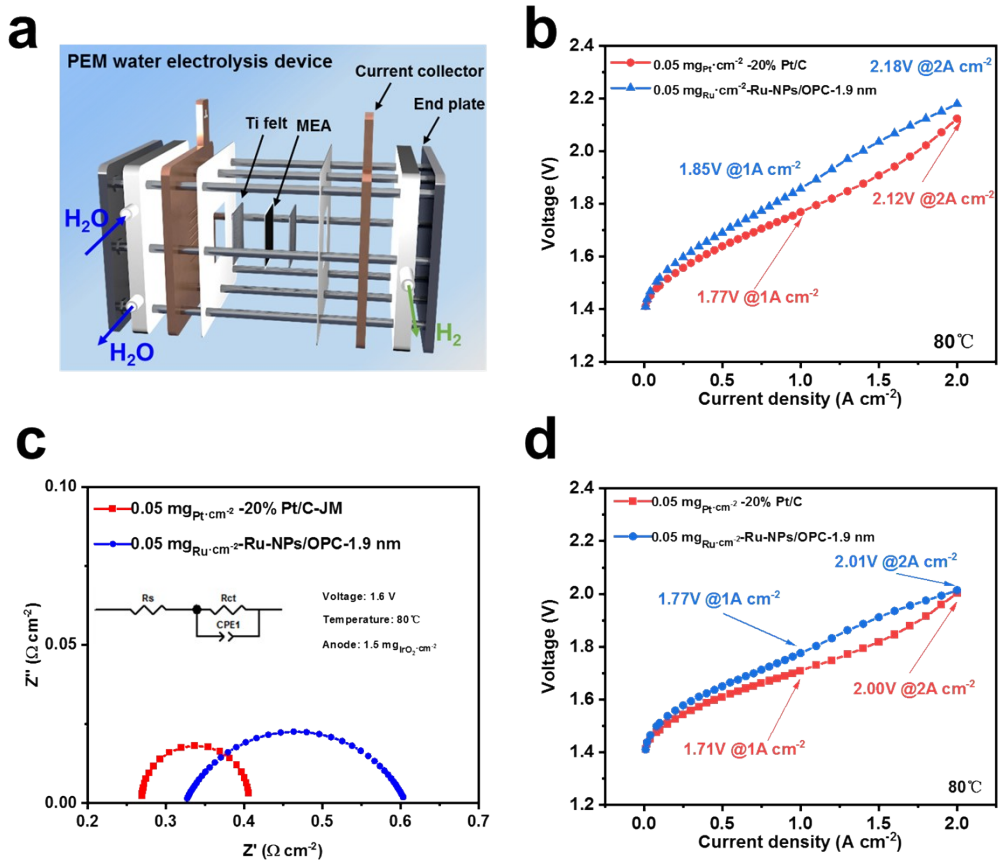

Figure S31. (a) Schematic of home-made PEM water electrolysis device. (b) Steady-state polarization curves without IR compensation, (c) EIS and (d) steady-state polarization curves with IR compensation for PEM water electrolysis of Ru-NPs/OPC-1.9 nm and 20% Pt/C as cathodic catalysts and with similar precious metal loadings.

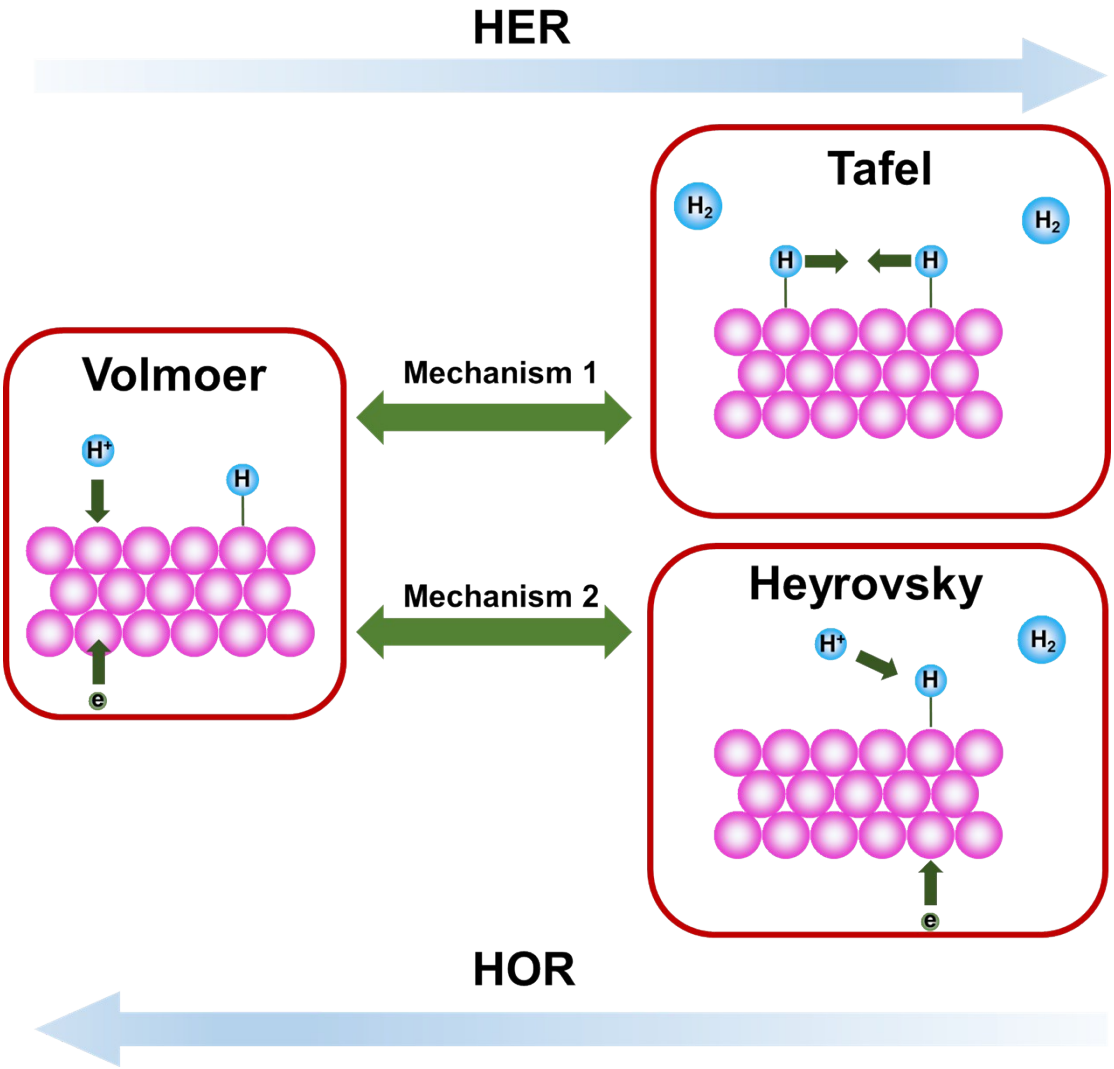

Figure S32 Schematic diagram of mechanism on hydrogen electrode reaction.

The HER and the HOR have incomplete symmetry. For HER, the first step is the Volmer reaction, where an electron flowing through the electrode combines with a proton from the solution, forming an adsorbed hydrogen on the active site of the electrode surface. Subsequently, the adsorbed hydrogen may finish the HER process along the Tafel step (The coupling of two neighboring adsorbed hydrogen and release hydrogen) or Heyrovsty step (The coupling of an adsorbed hydrogen, a new electron and a proton from the solution then release hydrogen). For HOR, the first step is the inverse process of Tafel or Heyrovsty step, then through the Volmer step to release proton. In general, for the HER and the HOR, the Volmer step is an inevitable process and the incomplete symmetry is derived from the Tafel or Heyrovsty step in the reaction.

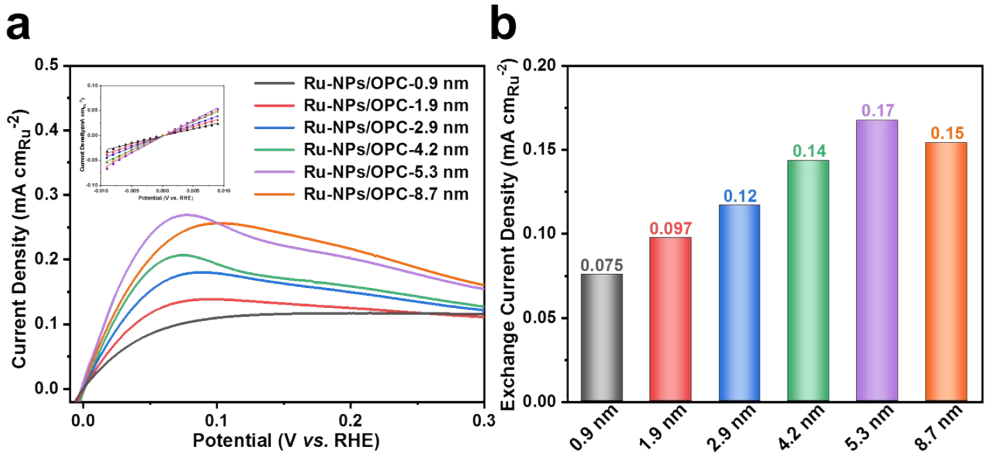

Figure S33. HOR activity analysis of Ru-NPs/OPC-X nm based on specific surface area. (a) LSV curves in 0.1 M $HClO_4$ aqueous solution saturated by H_2. Sweep rate: 10 mV s^{-1}; temperature: 25 °C. (b) Corresponding exchange current density of Ru-NPs/OPC-X nm.

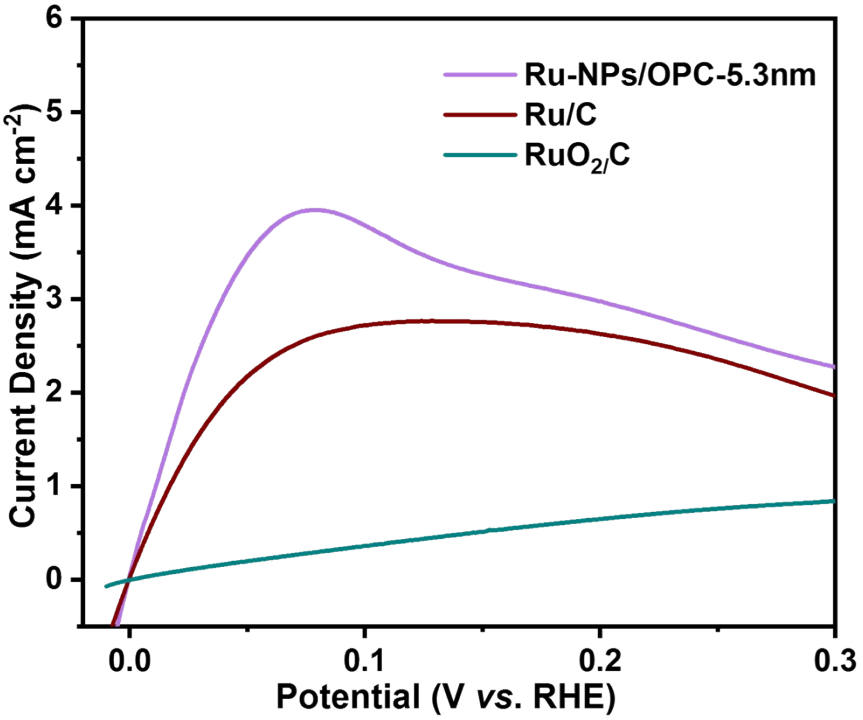

Figure S34. HOR polarization curves on Ru-NPs/OPC, Ru/C and RuO_2/C.

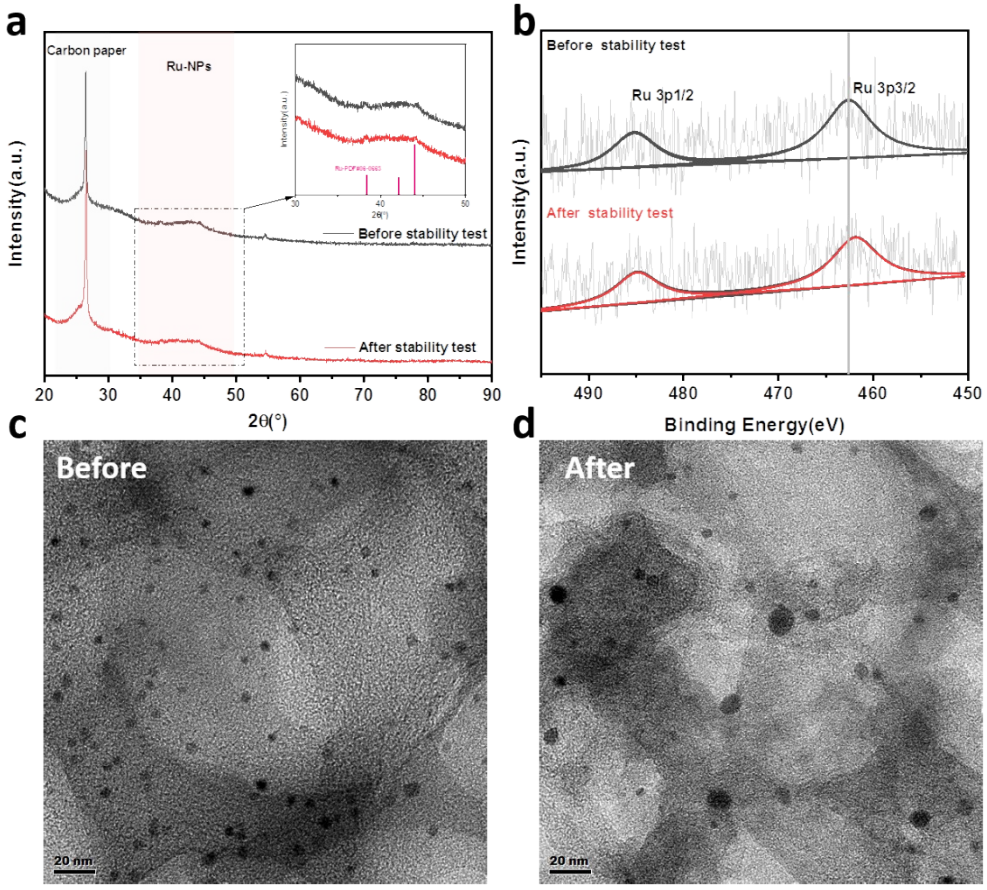

Figure S35. (a) XRD patterns, (b) XPS spectra and (c, d) TEM images before and after HOR stability test.

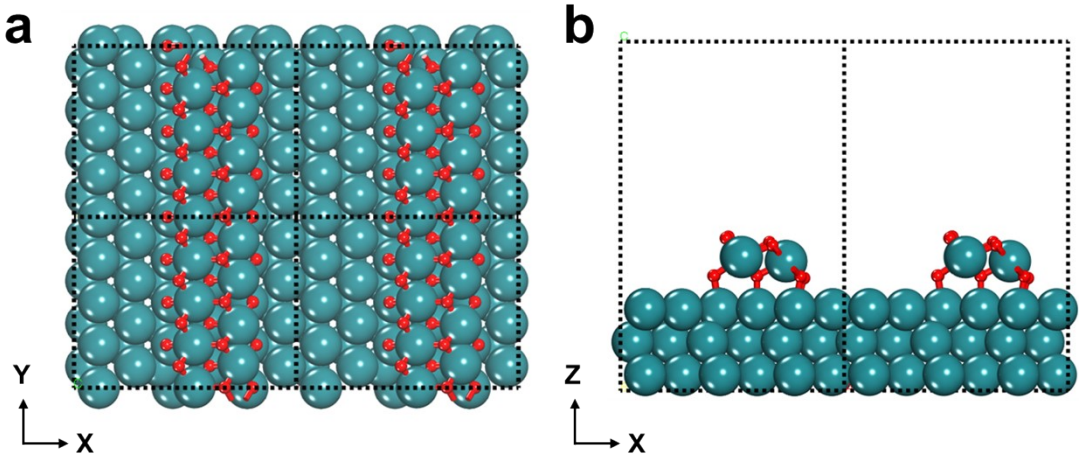

Figure S36. (a)Top view and (b) side view of the interface model of Ru-RuO_2.

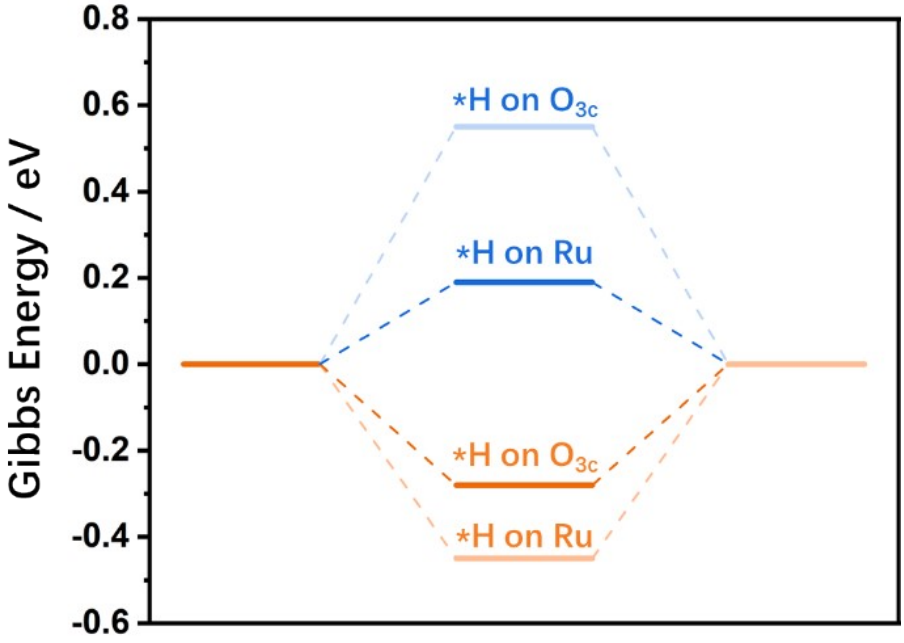

Figure S37. Adsorption free energies of hydrogen over tri-coordinated oxygen (O_{3c}) and ruthenium (Ru) for RuO_2 (blue line) and Ru-RuO_2 (orange line). It can be found that the Ru site is more active over protonated RuO_2, while the tri-coordinated oxygen site is more active over protonated Ru-RuO_2.

Table S1. BET surface areas of Ru-NPs/OPC-X nm, pure OPC and C-Ru-NPs.

Sample	BET Surface Area/$m^3 g^{-1}$
C-Ru-NPs	1450.2
Pure OPC	631.2
Ru-NPs/OPC-X nm	486.6

Table S2. Ru contents within Ru-NPs/OPC-X nm.

Catalyst	Ru content(wt.%)
Ru-NPs/OPC-0.9 nm	2.48
Ru-NPs/OPC-1.9 nm	2.00
Ru-NPs/OPC-2.9 nm	1.63
Ru-NPs/OPC-4.2 nm	1.61
Ru-NPs/OPC-5.3 nm	1.46
Ru-NPs/OPC-8.7 nm	1.24

Table S3. Linear component fitting (LCF) analysis of typical samples.

Sample	Weight of standards		Valance	R factor
	Ru foil	RuO_2		
Ru-NPs/OPC-1.9 nm	0.297±0.034	0.703±0.034	+2.8	0.027
Ru-NPs/OPC-2.9 nm	0.498±0.029	0.502±0.029	+2.0	0.018
Ru-NPs/OPC-5.3 nm	0.713±0.026	0.287±0.026	+1.2	0.018

Table S4. EXAFS fitting parameters at the Ru K-edge for various samples（S_0^2=0.82）

Sample	Shell	N[a]	R(Å)[b]	$\sigma^2\times10^3$(Å^2)[c]	ΔE_0 (eV)[d]	R factor
Ru foil	Ru-Ru	12*	2.68±0.01	3.9±0.3	-3.5±0.7	0.003
RuO_2	Ru-O	5.0±0.9	1.96±0.01	2.7±1.7	0.0±2.3	0.011
	Ru-Ru	5.2±3.1	3.18±0.04	18.8±7.1	-2.5±3.8	
	Ru-Ru	5.6±3.8	3.52±0.02	2.7±4.2		
Ru-NPs/OPC-1.9 nm	Ru-N	5.5±1.1	1.99±0.01	5.9±2.0	-2.8±2.6	0.006
	Ru-Ru	1.9±0.7	2.69±0.01	3.3±2.5	-1.3±2.7	
Ru-NPs/OPC-2.9 nm	Ru-N	5.3±2.4	1.98±0.03	9.7±4.7	-4.2±5.9	0.009
	Ru-Ru	4.4±1.0	2.65±0.01	4.5±1.3	-4.1±2.0	
Ru-NPs/OPC-5.3 nm	Ru-Ru	4.8±0.9	2.64±0.01	1.8±0.9	-8.7±2.1	0.013

[a]*N*: coordination numbers; [b]*R*: bond distance; [c]σ^2: Debye-Waller factors; [d] ΔE_0: the inner potential correction. *R* factor: goodness of fit.

Table S5. Geometric/specific surface areas, Ru loadings and ECSAs calculated via CuUPD.

Size (nm)	Geometric surface area (cm^2)	Specific surface area (cm^2)	Loading mass (ug)	ECSA (m^2/g)
0.9	0.196	4.23	3.97	107
1.9	0.196	4.04	3.20	126
2.9	0.196	3.46	2.61	133
4.2	0.196	3.27	2.58	127
5.3	0.196	2.88	2.34	123
8.7	0.196	2.21	2.00	106

Table S6. Formulation and conditions of different sizes PS microspheres.

Reagent\particle size	180nm	230nm	280nm	320nm
Styrene/ml	30	30	32.5	30
PVP/g	1.5	1	1.25	0.3
$K_2S_2O_8$/g	0.5	0.5	0.5	0.1
Temperature/°C	75	75	60	75
Scattering color	Green	Yellow	Blue	Purple

References

[1] H. Hong, J. Liu, H. Huang, C. Atangana Etogo, X. Yang, B. Guan, L. Zhang, *J. Am. Chem. Soc.* **2019**, 141, 14764.

[2] H. Zhang, S. Hwang, M. Wang, Z. Feng, S. Karakalos, L. Luo, Z. Qiao, X. Xie, C. Wang, D. Su, Y. Shao, G. Wu, *J. Am. Chem. Soc.* **2017**, 139, 14143.

[3] a) G. Kresse, J. Furthmüller, *Comput. Mater. Sci.* **1996**, 6, 15; b) G. Kresse, J. Furthmüller, *Phys. Rev. B* **1996**, 54, 11169.

[4] a) P. E. Blöchl, *Phys. Rev. B* **1994**, 50, 17953; b) G. Kresse, D. Joubert, *Phys. Rev. B* **1999**, 59, 1758.

[5] J. P. Perdew, K. Burke, M. Ernzerhof, *Phys. Rev. Lett.* **1996**, 77, 3865.

[6] A. A. Peterson, F. Abild-Pedersen, F. Studt, J. Rossmeisl, J. K. Nørskov, *Energy Environ. Sci.* **2010**, 3, 1311.

[7] T. Wang, H. Xie, M. Chen, A. D'Aloia, J. Cho, G. Wu, Q. Li, *Nano Energy* **2017**, 42, 69.